

ASHUTOSH SHARMA<sup>1</sup>, MYOUNG JIN CHAE<sup>1</sup>, BYUNGMIN AHN<sup>1\*</sup>

## BRAZEABILITY AND MICROSTRUCTURE OF Ag-28Cu MICROJOINING FILLER PRODUCED BY HIGH ENERGY BALL MILLING

In this paper, we have studied the evolution of morphology and brazing behavior of Ag-28Cu alloy filler processed by high energy ball milling. The milling of the powder mixture was carried out for 40 h. The structural and morphological analyses were performed by the X-ray diffraction and scanning electron microscopy. The melting temperature of the braze filler was determined by differential thermal analysis. The filler wetting properties were assessed from the spread area ratio measurements on various Ti substrates. The results indicate that the ball milling can effectively depress the filler melting point and enhance the brazeability. The milled powder mixture showed Ag(Cu) solid solution with a crystallite size of 174-68 nm after 40 h. It was shown that the high energy ball milling can be a potential method to develop low temperature brazing fillers for advanced microjoining applications.

*Keywords:* filler, microjoining, dissimilar, ball milling, microstructure

### 1. Introduction

With the advancement of structural materials, there is always a need to join two different classes of materials for specific applications. For example, microjoining of the ceramics to metals in power modules, dental implants, actuators, relay device contacts, and other areas. These dissimilar materials are joined by specialized fillers known as brazing fillers [1]. Brazing fillers enhance the wetting of the contact surfaces and make the joining possible via diffusion bonding. There are various kinds of brazing fillers for various microjoining applications, for example, BA1, BCu, BNi, BAg, etc. [2-4]. However, most popular brazing fillers are devoted to the BAg group due to their special ability to join ceramic and metals [5]. BAg type fillers generally contain Ag-Cu in eutectic composition. Further addition of elements like Ti, Sn, Zr to Ag-28Cu alloy has also been reported to enhance the wetting or brazed joint characteristics. However, too much addition of the metallic elements imposes serious concern over the reliability of the joint [6]. In addition, there is a possibility of the formation of multiple intermetallic compounds (IMCs) after the addition of numerous elements to the eutectic Ag-Cu alloy. These multiple IMCs may increase the joint residual stresses and may lead to failure of the entire device [6-7]. In literature, most of the investigations are concentrated

on the study of microstructure, mechanical and thermodynamic properties Ag-Cu alloys [8-10]. Various researchers have added ceramic nanoparticles to the Ag-Cu matrix to control the thermal and microstructural properties required for low-temperature brazing. Most of the brazing industries always look for the filler that operates at lower temperatures for economic reasons. However, the use of secondary reinforcements is not desirable due to the dispersion and melt segregation issues during brazing [1-6]. It can be seen from the past literature that the study on the nanostructured Ag-Cu is limited which can be a potential low-temperature filler relative to the conventional Ag-Cu filler.

Therefore, research on the development of nanostructured Ag-Cu alloys is in high demand. Various brazing fillers are prepared by different methods such as melting and casting, powder metallurgy, plating, vapor deposition methods, chemical methods, and high energy ball milling (HEBM). Each one of the methods has its own benefits and drawbacks. For example, melting and casting methods need high-temperature control and induce undesirable pores and casting defects after solidification. Powder metallurgy and vapor deposition methods are faster but require expensive tools and machines. In addition, precise control of the environment (Ar, N<sub>2</sub> or Vacuum) is needed during the fabrication process. The chemical methods including plating are simple but involve the use of hazardous chemicals. The handling

<sup>1</sup> AJOU UNIVERSITY, DEPARTMENT OF MATERIALS SCIENCE AND ENGINEERING AND DEPARTMENT OF ENERGY SYSTEMS RESEARCH, 206 WORLDCUP-RO, YEONGTONG-GU, SUWON, GYEONGGI, 16499, KOREA

\* Corresponding author: byungmin@ajou.ac.kr



of chemicals requires great care which is associated with toxicity and waste disposal issues. Among various methods, HEBM seems to be an appropriate method for the production of the fillers due to its simplicity and easy fabrication approach [11]. Moreover, the HEBM approach can produce novel microstructures for better uniformity in composition [12]. The formation of nanostructure in the alloy can also bring down the melting temperature to a very low value which can be beneficial for saving time and energy during the brazing operation.

Therefore, in this work, we have attempted the fabrication of the Ag-28Cu alloy via the HEBM approach. We also characterized and evaluated the effect of HEBM on the wetting and melting behavior of the Ag-28Cu filler.

## 2. Experimental

The materials used for the preparation of brazing filler via HEBM consists of pure Ag and Cu powder procured from the Loba Chemie, India. The compositions of the filler composition selected for the study (Table 1).

TABLE 1

Experimental composition of the Ag-Cu filler

Element	Composition (wt.%)	
	Ag	Cu
Values	72	28

The powders were chosen in eutectic composition and subjected to milling for 40 h in a Retsch planetary ball mill for 40 h. The ball to powder charge ratio was 10:1 and the milling media contained 50 balls of WC in WC vials. About 0.2 wt% stearic acid was mixed with the powder mixture to avoid the cold welding of the particles during the HEBM process. Table 1 shows the composition of the powders chosen in this work.

The HEBMed powder was characterized for the particle size and phase evolution by X-ray diffraction machine (XRD, benchtop, Miniflex, Rigaku, Japan). The crystal size and the induced lattice strain were estimated by the Scherer method. The sample preparation for XRD was done according to the standard practice. The sample was pasted on the glass slide holder (10 mm × 10 mm × 2 mm). All the powder samples were handled with great care to avoid even minute contamination from the external environment. The measurements were carried out at 35 kV and 35 mA operating parameters with a copper cathode ( $\lambda(K\alpha) = 1.54056 \text{ \AA}$ ). All the samples were scanned from 20 to 90°. Further analysis was carried out to compute the crystallite size and lattice strain induced in the powder particles.

The morphology of the powder after milling was examined by the scanning electron microscope (SEM). The compositional analysis was carried out by the energy-dispersive X-ray spectroscopy (EDS) together with SEM.

The melting point of the filler powders was evaluated by differential thermal analyser (DTA Perkin, Elmer, STA 8000)

from 50-900°C at a heating rate of 10°C. The alumina pans were used for heating and Ar gas was used as the inert environment during the experiment.

The filler brazeability was estimated by reflowing the filler powder over the Ti substrate at 850°C for 4 min and estimating the area change after solidification. The area ratio was calculated and reported as an estimate of the brazeability.

## 3. Results and discussion

The phase evolution of the Ag-28Cu filler alloy after HEBM was observed by XRD analysis as shown in Fig. 1. Various peaks are related to Cu and Ag solid solutions. The peak positions of Cu and Ag do not differ significantly with each other, however, the shifting of the peaks is noticed. This observation indicates the formation of the Ag(Cu) solid solution [13]. The solid solution appeared after 40 h of milling at  $2\theta = 39.2^\circ$ . This indicates the formation of nanosized domains and the introduction of lattice defects. The average particle size of the Ag and Cu phase was estimated by full width half maximum method using Williamson-Hall (W-H) method. The average particle size of the Ag-28Cu alloy after 40 h ball milling was determined to be around 68 nm according to the W-H method as follows [14]:

$$\beta(hkl) \cos\theta = 0.9\lambda/D + 4\varepsilon \sin\theta \quad (1)$$

Assuming Cauchy distribution, the wavelength of the X-rays,  $\lambda = 1.5406 \text{ \AA}$ ,  $\theta$  denotes the diffraction angle.  $D$  and  $\varepsilon$  denote the average particle size and lattice strain. The instrumental error can be removed by the relation,  $\beta^2(hkl) = \beta^2_{\text{measured}} - \beta^2_{\text{instrument}}$ , where  $\beta$  = full width at half maximum. The average particle size and lattice strain with various milling times are summarized in Table 2. The particle size of Ag and Cu decreases continuously to a minimum of 68 nm after 40 h milling [15]. The induced lattice strain was also found to increase due to the heavy deformation of the crystal lattice after milling. A decrease in the crystallite size of the filler is beneficial for the brazing. High surface energy Ag-28Cu nanopowder is expected to have lower the melting point and improve wettability.

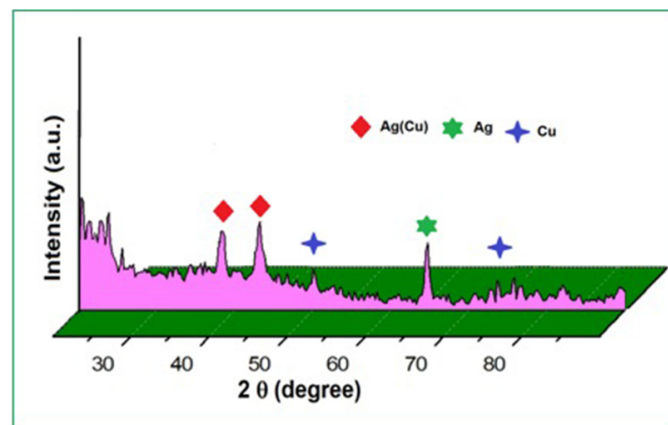


Fig. 1. XRD pattern of the Ag-28Cu filler after milling for 40 h

TABLE 2

Crystallite size and lattice strain

Milling time (h)	Crystallite size (nm)	Lattice strain (%)
5	174	0.0026
10	168	0.0037
20	152	0.0051
30	116	0.0163
40	68	0.0190

The surface morphology of the Ag-28Cu powders was observed under the SEM machine (Fig. 2). Initially, the bigger particles were broken down into fine fragments [12]. These fragments get cold-welded in due course until 20 h milling and undergo work hardening before attaining nanocrystal size of 68 nm after 40 h of milling. The compositional analysis was performed by the EDS measurements which confirm the presence of the Ag, Cu and the formation of Ag(Cu) solid solution in the lattice. The compositional analysis is tabulated in Table 3 which confirms a near eutectic Ag-Cu solid solution.

TABLE 3

Compositional analysis of Ag-28Cu filler

Phase	Composition (wt.%)	
	Cu	Ag
Bright	33	67
Dark	88	12

A typical DTA curve after 40 h of milling is shown in Fig. 3. It was noticed that the filler melting temperature decreased

significantly after HEBM. In accordance with the binary phase diagram, the eutectic melting point of Ag-28Cu alloy is around 780°C [6]. The final solidus temperature after HEBM of 40 h was found to be about to 778.6°C which is very close to the standard Ag-28Cu alloy. We also presented the DTA curves of Ag-Cu alloy for various milling times. The various melting temperatures (solidus, liquidus, and pasty range) are presented in Table 4. It can be seen that there is a continuous decrease in the melting temperatures with increasing milling times. This was possible due to the progressive reduction of the nanocrystal size after prolonged milling times. The formation of nanocrystals is associated with the lowering of the Gibbs free energy and hence lower energy is needed to fully melt the crystal lattice [12]. Previous reports have established that the melting enthalpy follows the inverse relation with the grain size which confirms the fact that stored energy during milling is increased significantly at higher milling times [15]. In addition, the solidus to liquidus range, i.e., the pasty range is  $\approx 7.8^\circ\text{C}$  after 40 h of HEBM. It has been reported that a pasty range  $< 10^\circ\text{C}$  is beneficial for brazing

TABLE 4

Various melting temperatures obtained from the thermal analysis

Milling time (h)	T (solidus, °C)	T (liquidus, °C)	Pasty range (liquidus-solidus, °C)
5	779.8	789.4	9.6
10	779.5	788.7	9.2
20	779.1	787.8	8.7
30	778.2	786.9	8.7
40	778.6	786.4	7.8

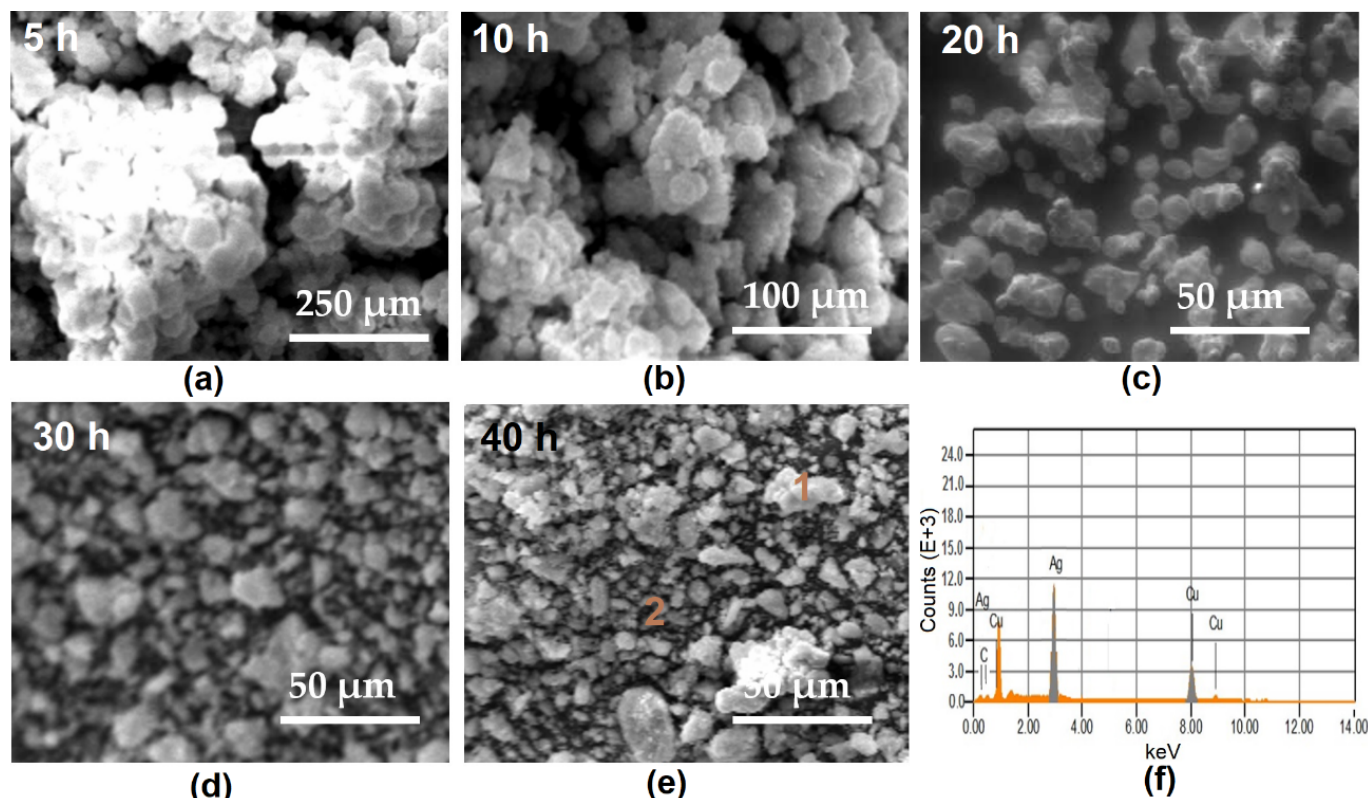


Fig. 2. SEM micrograph of Ag-28Cu alloy powder milled for various times and EDS analysis

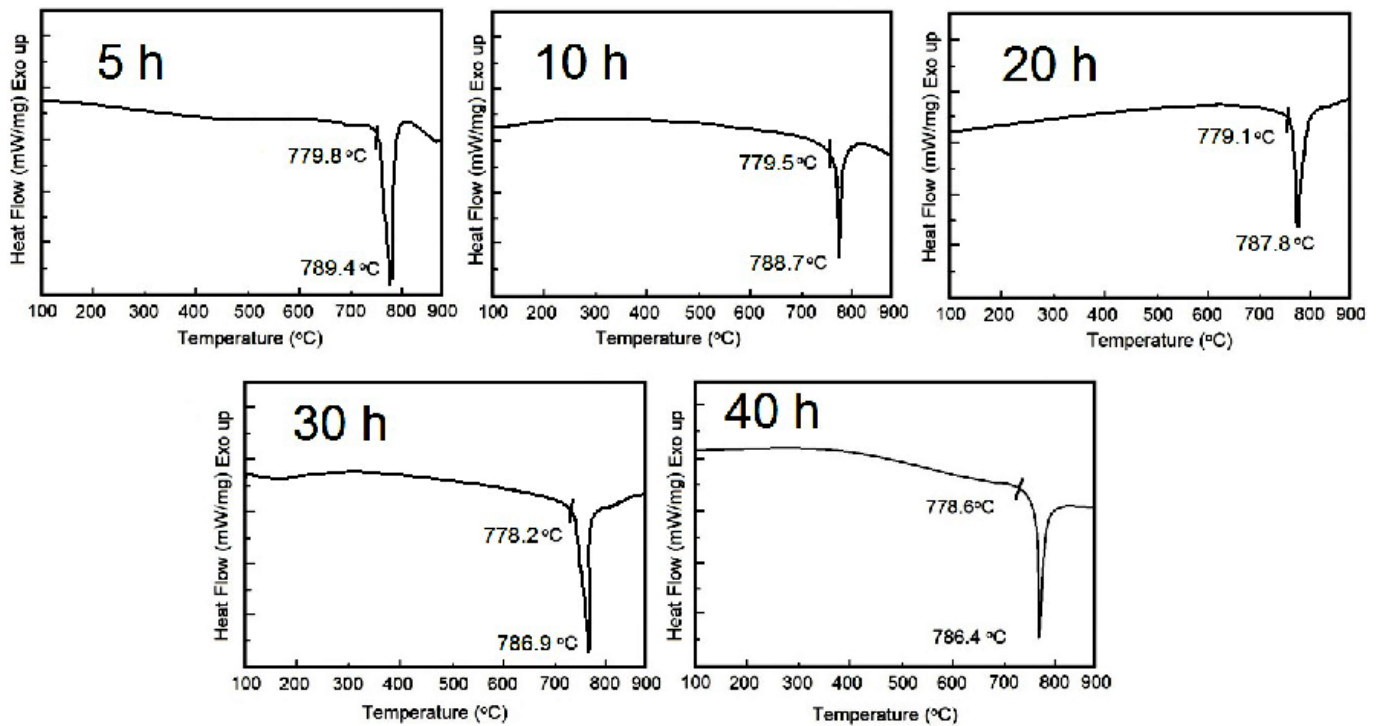


Fig. 3. Melting temperatures of the HEBMed Ag-28Cu filler alloy after various milling times

operations to avoid the thermal fluctuations (shrinkage pores or hot tear) in the joint [16].

To estimate the filler brazeability, area spread ratios were recorded after reflowing the filler powder at 850°C. The spreading was recorded on a Ti substrate for 220 s. The area spread ratio was calculated by the equation [17-18]:

$$\text{Spread ratio (\%)} = (\Delta A) / A_i \quad (2)$$

Here,  $\Delta A = A_f - A_i$  is an area ratio difference before and after spreading. The adopted reflow profile for the filler spreading is shown in Fig. 4. The spread area ratios improve with the HEBM due to the availability of high surface areas which accelerate the melting and spreading of the powder on the substrate [4,6,19,20]. The spreading ratio was plotted in Fig. 5. The spread ratio was

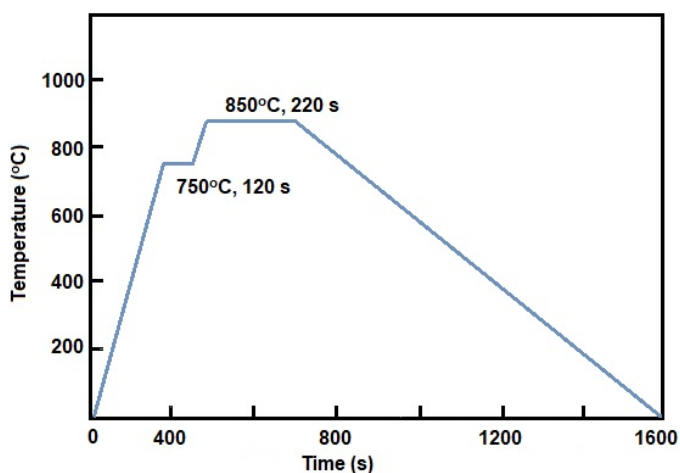


Fig. 4. The reflow profile for the measurement of the brazeability of the Ag-28Cu alloy powder

lowest for the Ag-Cu milled for up to 10 h and increased rapidly beyond 30 h due to the rapid nanostructuring of the powder particles. The spread ratio was highest at around 96% after milling time of 40 h (Fig. 5).

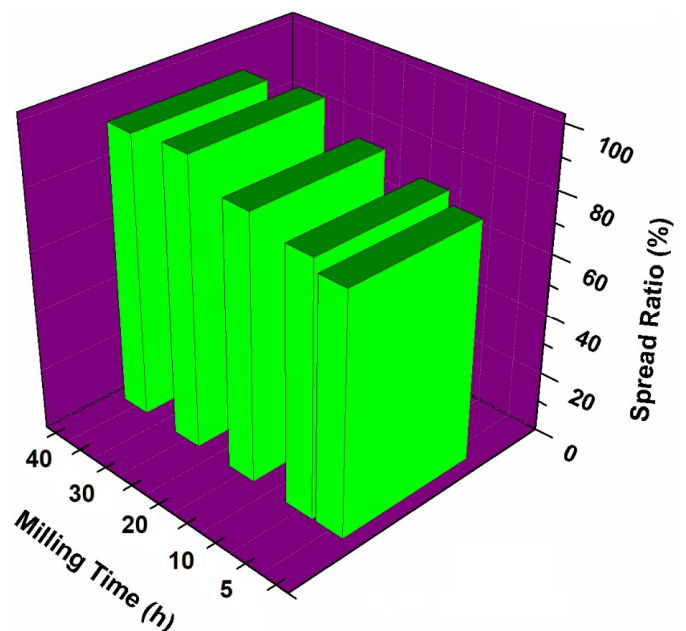


Fig. 5. The brazeability of the Ag-28Cu powder after various milling times

In general, the spreading of a brazing filler depends upon various intermolecular forces of attraction that operate at the solid-liquid-vapor boundaries. According to Young's equation of wettability, the ability of a filler to spread and make inti-

mate contact with the contact surface is given by the relation [11]:

$$\frac{\gamma_{sv} - \gamma_{sl}}{\gamma_{lv}} = \cos \theta \quad (3)$$

where,  $\gamma_{sv}$ ,  $\gamma_{lv}$ , and  $\gamma_{sl}$  display the various interfacial energies at the interface (solid-vapor, liquid-vapor, and solid-liquid interface). The wetting angle is given by  $\theta$ . Alternatively, from equation (3), the spreading parameter (S) can be given by [11]:

$$S = \gamma_{sv} - (\gamma_{sl} + \gamma_{lv}) \quad (4)$$

So that,  $S > 0$  for appreciable wetting,  $\theta < 90^\circ$

$S < 0$  for partial wetting,  $\theta > 90^\circ$

From the equations, (3) and (4), it can be seen that a smaller value of wetting angle  $\theta$  indicates higher spreading. Therefore, there is a positive effect on spreadability after HEBM of Ag-Cu alloy powder. A continuous nanostructuring will lead to a decrease in the interfacial energy at the contact surfaces and hence will bring down the wetting angle according to equation (3). Therefore, we see an improvement in the spreadability of the Ag-Cu powder after 40 h of ball milling.

In advanced microjoining applications, especially for ceramic and metal bonding, such as dental implants, thermoelectric power module joining or in transducers, a reasonable spreading of the filler is desired for better integration of the entire device. All these observations show that HEBM is an essential tool for the preparation of nanosized fillers with high wetting, excellent microstructure and melting properties [7,11]. Thus HEBM can be a potential strategy for developing the robust brazing process.

#### 4. Conclusions

HEBM of the Ag-28Cu alloy was performed in this study. It was shown that the solid solution formation occurred in Ag-28Cu filler alloy after 30 h of ball milling which was identified by the peak shifts in the XRD patterns. The powder particle size was considerably refined after milling from 174 nm to 68 nm. The microstructure of the powder showed the formation of big lumps but which turned finer after prolonged milling. The melting temperature of the Ag(Cu) solid solution was found to be 778.6°C. It was also found that the filler spreadability of the composite powder was significantly improved. The spread ratio of the filler was improved from 72% to 96% after milling up to 40 h.

#### Acknowledgments

This research was supported by Basic Science Research Program through the National Research Foundation of Korea (NRF) funded by the Ministry of Education (NRF-2018R1D1A1B07044481) (B.A.). This research was supported by Basic Science Research Program through the National Research Foundation of Korea (NRF) funded by the Ministry of Education (NRF-2018R1D1A1B07044706) (A.S.).

#### REFERENCES

- [1] A.K. Srivastava, A. Sharma, Am. J. Mater. Eng. Technol. **5** (1), 7-13 (2017).
- [2] A. Sharma, S.H. Lee, H.O. Ban, Y.S. Shin, J.P. Jung, JWJ **34** (2), 30-35 (2016).
- [3] A. Sharma, S.J. Lee, D.Y. Choi, J.P. Jung, J. Mater. Proc. Technol. **249**, 212-220 (2017).
- [4] A. Sharma, S.J. Lee, J.H. Oh, J.P. Jung, Korean J. Met. Mater. **55** (12) 836-844 (2017).
- [5] A. Sharma, S.H. Kee, F. Jung, Y. Heo, J.P. Jung, J. Mater. Eng. Perform. **25** (5), 1722-1728 (2016).
- [6] J. Shin, A. Sharma, D.H. Jung, J.P. Jung, J. Met. Mater. **56** (5), 366-374 (2018).
- [7] A. Sharma, X. Di, J.P. Jung, Mater. Res. Exp. **6** (5), 056526 (2019).
- [8] Z.Q. Li, T.B. Chen. Mater. Charact. **49**, 67-72 (2002).
- [9] J. Lin, L. Meng. J. Alloys Compd. **454**, 150-155 (2008).
- [10] F. Delogu. Mater. Chem. Phys. **115**, 641-644 (2009).
- [11] S. Mishra, A. Sharma, D.H. Jung, J.P. Jung, Met. Mater. Int. (2019), DOI: 10.1007/s12540-019-00536-4 (in press).
- [12] C. Suryanarayana, Prog. Mater. Sci. **46** (1-2), 1-184 (2001).
- [13] L. Li, T. Qiu, J. Yang, Y. Feng, Adv. Mater. Res. **92**, 271-276 (2010).
- [14] V.D. Mote, Y. Purushuttom, B.N. Dole, J. Theor. Appl. Phys. **6**, 1-8 (2012).
- [15] B. Reddy, P. Bhattacharya, B. Singh, K. Chattopadhyay, J. Mater. Sci. **44**, 2257-2263 (2009).
- [16] A. Sharma, B. Ahn, Adv. Mater. Sci. Eng. **2019**, 1-11 (2019).
- [17] A. Sharma, A.K. Srivastava, B. Ahn, Metall. Mater. Trans. A **50** (11), 5384-5394 (2019).
- [18] A. Sharma, H. Yu, I.S. Cho, H. Seo, B. Ahn, Electron. Mater. Lett. **15** (1), 27-35 (2018).
- [19] A. Sharma, M.H. Roh., D.H. Jung, J.P. Jung, Metall. Mater. Trans. A **47A**, 510-521 (2016).
- [20] A. Sharma, D. Lim, J.P. Jung, Mater. Sci. Technol. **32**, 773-779 (2016).